Segmental Dynamics of Head-to-Head Polypropylene and Polyisobutylene in Their Blend and Pure Components

Ernest Krygier,[||] Guoxing Lin, Jessica Mendes, Gatambwa Mukandela, David Azar, and Alan A. Jones*

Carlson School of Chemistry and Biochemistry, Clark University, Worcester, Massachusetts 01610

Jai A. Pathak,[†,§,||] Ralph H. Colby,[‡] and Sanat K. Kumar[⊥,‡]

Departments of Chemical Engineering and Materials Science and Engineering, The Pennsylvania State University, University Park, Pennsylvania 16802

George Floudas[#]

Foundation for Research and Technology - Hellas (FORTH), Institute of Electronic Structure and Laser (IESL), P.O. Box 1527, 711 10 Heraklion, Crete, Greece

Ramanan Krishnamoorti

Department of Chemical Engineering, University of Houston, Houston, Texas 77204

Rudolf Faust

Department of Chemistry, University of Massachusetts, Lowell, Massachusetts 01854

Received August 30, 2004; Revised Manuscript Received April 12, 2005

ABSTRACT: Segmental dynamics are measured in pure polyisobutylene (PIB), pure deuterium-labeled head-to-head poly(propylene) (hhPP), and a blend containing 70% PIB/30% hhPP by mass using ^{13}C spin−lattice relaxation, ^{2}H spin−lattice relaxation, and dielectric spectroscopy (DS). The NMR measurements are made between 313 K and 413 K (spin−lattice relaxation measurements are sensitive to motions in the nanosecond range), while the DS measurements (which span the second to microsecond range) are made between 225 K and 325 K. While NMR and DS monitor local dynamics over a wide range of temperature and time, NMR has the additional advantage of being able to determine the local motion of *each component* in the blend through isotopic labeling. The spin−lattice relaxation data are interpreted using a modified Kohlrausch−Williams−Watts (KWW) correlation function with a Vogel−Fulcher−Tammann−Hesse (VFTH) temperature dependence of relaxation time, giving temperature-dependent segmental correlation times from NMR in the short time (high temperature) range that are compared to dielectric segmental correlation times at lower temperatures. Because of the small PIB dipole moment, DS on hhPP/PIB blends is dominated by the dynamics of hhPP. NMR measurements show very little shift in the component dynamics upon blending, but the shift becomes larger at lower temperatures. One factor in the variation of the separation between the dynamics of the two polymers with temperature is the unusual VFTH parameters for pure PIB, which signify its small fragility. The Lodge−McLeish model is unsuccessful in predicting the changes in component dynamics upon blending for hhPP, while it describes the temperature-dependent dynamics of PIB over the limited temperature range studied by NMR.

Introduction

The blending of polymers can be used to adjust properties relative to the components for specific technological applications.[1] Some important properties depend on the dynamics of the polymer backbones that are altered by blending. Despite a number of efforts to understand changes in dynamics upon blending,[2−23] it is still difficult to *predict* blend dynamics based solely on information on the pure components. Local segmental dynamics in a limited number of systems have been studied in detail, and the changes in dynamics vary widely from system to system. In a blend of polystyrene and poly(phenylene oxide),[6,7] the glass transition temperatures of the components differ by 125 K, corresponding to orders of magnitude differences in the time scale of motion at a given temperature, yet the motions are almost coincident in the blend. At the other extreme, the local segmental dynamics in a blend of poly(ethylene oxide) and poly(methyl methacrylate) differ by about 12 orders of magnitude.[15−17,23] In the well-studied blend of polyisoprene (PI) and poly(vinyl ethylene) (PVE), the local dynamics of the components approach each other but nevertheless remain distinct.[10,11,18,22]

A number of factors have been considered in an attempt to predict changes in dynamics produced by blending.[11,14,19−21] The intrinsic dynamics of the chains are a typical starting point with the amount of change in the dynamics depending on coupling between the chains, self-concentration effects, and composition fluctuations. Recent models focusing on concentration variations have had some success and in particular the self-concentration model of Lodge and McLeish[21] (henceforth referred to as the "LM model") can readily yield a

[†] Department of Chemical Engineering.
[‡] Department of Materials Science and Engineering.
[§] Current address: Polymers Division, National Institute of Standards and Technology, Gaithersburg, MD 20899-8544.
[⊥] Current address: Department of Chemical Engineering, Rensselaer Polytechnic Institute, Troy, NY 12180.
[#] Current address: Department of Physics, University of Ioannina, Ioannina, Greece 45110.
[||] These authors contributed equally to this work.

10.1021/ma048224f CCC: $30.25 © 2005 American Chemical Society
Published on Web 08/06/2005

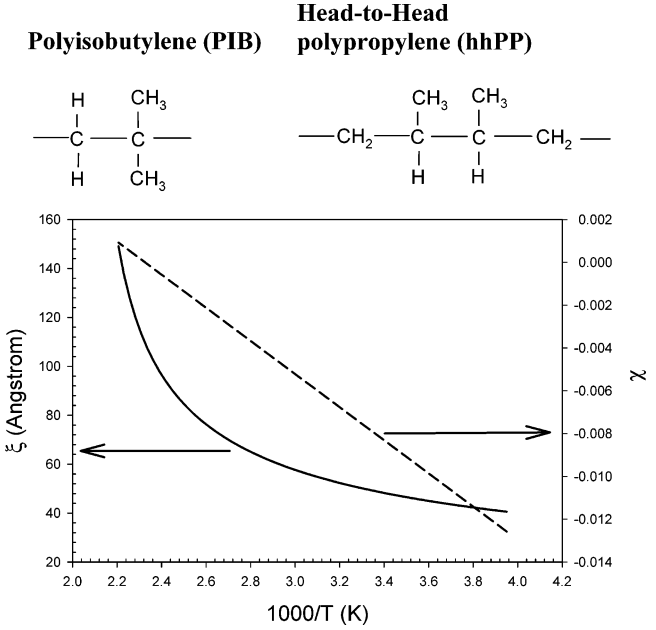

Figure 1. (a, top) Repeat unit structures of PIB and hhPP. (b, bottom) Flory χ parameter (reported by Krishnamoorti et al.[24] using SANS experiments) and correlation length ξ (mean-field estimate, calculated using χ) as a function of inverse temperature. The estimated average Kuhn segment length is 12 Å.[30]

prediction for comparison with observations. Part of the motivation for this study comes from recent NMR studies[22,23] on blends and the associated interpretation using the LM model.

The system selected for study here, polyisobutylene (PIB) and head-to-head poly(propylene) (hhPP), involves two relatively simple hydrocarbon backbones consisting of only carbon−carbon single bonds with methyl groups as side chains (see Figure 1a for structures). Relative to other saturated hydrocarbon blends, those with PIB have larger interaction energies.[24] There is no obvious source for the relatively large interaction energy between PIB and hhPP although the blend is miscible,[24] as evidenced by a (surprisingly) negative value of the Flory−Huggins χ parameter (measured by small-angle neutron scattering, SANS): $\chi = 0.018 - 7.74/T$, making $\chi = -0.01$ at $T = 273$ K (see Figure 1b). High molar mass PIB/hhPP blends have lower critical solution temperature (LCST) behavior with a critical temperature[24] of ∼460 K.

Spin diffusion NMR measurements performed by White and Lohse[25] indicate a "length scale of concentration fluctuations" ≤3.5 nm in the blend. This length scale is somewhat less than the correlation length for concentration fluctuations ξ in the blend, calculated on the basis of the SANS-determined χ parameter (see Figure 1b), using the mean-field estimate of

$$\xi = \sqrt{\frac{Nb^2}{12[1 - 2\chi N\phi(1-\phi)]}}$$

for a blend containing components with equal number of mers, N (assumed to be 1000 for each component in this calculation), and ϕ is the volume fraction of hhPP (= 0.5 in this calculation). We determine $\xi = 4.9$ nm at 298 K. Given the differences in assumptions between SANS and NMR, the two results for the length scale of concentration fluctuations are in reasonable agreement. NMR requires knowledge of the spin diffusion coefficient and an assumption about geometry. The smaller result from NMR may reflect the fact that a diffusion based measurement of size is biased towards the smallest dimension of a non-spherical object.

Only a small volume would be swept out by conformational events in either polymer, indicating little likelihood of significant intermolecular steric interactions. PIB itself is unusual in several ways. The temperature dependence of the dynamics in this polymer is weak with more of an Arrhenius character at elevated temperatures than a Vogel−Fulcher−Tammann−Hesse (VFTH) dependence.[26] The impermeability of PIB to gases as a rubber well above the glass transition temperature is attributed[27−29] to good intermolecular packing, reflected also in its higher density as compared to other polyolefins. The weak temperature dependence of the PIB dynamics combined with the likely more normal temperature dependence of the hhPP may lead to a merging or near merging of the time scales of segmental motion of the pure components at higher temperatures despite a glass transition temperature difference of 50 K. The situation differs from the other well-studied hydrocarbon blend[10,11,18,22] of PI and PVE where the dynamics of the two pure polymers have more comparable VFTH dependences.

To measure the local dynamics of the two polymers, a combination of NMR and dielectric spectroscopy (DS) data are reported. The local dynamics of hhPP and hhPP/PIB blends have hitherto not been reported in the literature. The strength of NMR is that the dynamics of each component in the blend can be individually observed by blending deuterated hhPP with protonated PIB. ^{2}H spin−lattice relaxation measurements are then used to characterize hhPP local motions in the blend, and ^{13}C spin−lattice relaxation is used to characterize PIB local motions in the blend and in both pure components. The limitation of spin−lattice relaxation as a method to characterize local motion is the modest accessible temperature range: in this case, 303 K−413 K. To augment the temperature range, DS is performed closer to T_g. We show that DS selectively probes the segmental dynamics of hhPP in the blend due to the higher dipole moment of hhPP as compared to PIB. Since spin−lattice relaxation is sensitive to motions in the nanosecond range while the dielectric data cover the microsecond to second range, DS and NMR data sets collectively span a temperature range of 200 K and 10 decades in time, thus providing a good basis for assessing the relationship between these two techniques and for elucidating the effects of blending on the segmental dynamics of hhPP and PIB and comparison with molecular models of segmental dynamics in miscible polymer mixtures.

Experimental Section

Sample Preparation and Thermal Characterization. The hhPP was prepared at the University of Houston using in vacuo anionic polymerization of 1,4-poly(2,3-dimethyl-1,3-butadiene) (PDMB) with *sec*-butyllithium initiator, degassed methanol terminating agent, and cyclohexane solvent. PDMB was saturated in cyclohexane using $Pd/CaCO_3$ catalyst (20.4 atm hydrogen pressure, ∼380 K). Partially deuterated hhPP was prepared by using D_2 gas instead of H_2 gas. Repeated saturation was done on PDMB using a 3:1 catalyst−polymer ratio. The hhPP contained less than 3% residual unsaturation as checked by solution NMR. For both protonated and deuterated forms of hhPP $M_w = 3.0 \times 10^4$ with $M_w/M_n < 1.08$.

Solution deuterium NMR indicates the deuterium is inserted in methyl and backbone positions.

The deuterated hhPP used in the NMR measurements and the hydrogenated hhPP used in the dielectric measurements are both prepared from the same sample of PDMB. In the first case D_2 gas is used to saturate the double bond, and in the second case H_2 gas is used to saturate the double bond. This should lead to nearly identical hhPP for both studies eliminating any uncertainty associated with the use of different hhPP samples in the two measurements.

The PIB blended with hhPP in this study was obtained by fractionation[30] of a polydisperse commercial PIB (Scientific Polymer Products, Ontario, NY). The M_w of this PIB fraction is 6.13×10^5 with $M_w/M_n < 1.2$. Since sufficient mass of this particular PIB fraction was not available for both pure component and blend studies of both terminal and segmental dynamics,[30] another PIB sample (prepared at University of Massachusetts−Lowell using living cationic polymerization) having $M_w = 2.18 \times 10^5$ and $M_w/M_n = 1.18$ was used for DS on pure PIB only.

A blend consisting of 30% mass fraction hhPP and 70% mass fraction PIB was prepared by first making 1% solutions of the polymers in cyclohexane and blending the solutions after dissolution. The solvent was flashed in a rotary evaporator and then dried to constant mass under vacuum at 333 K in about 4 weeks. The glass transition temperature (T_g) of the pure polymers was determined by differential scanning calorimetry (DSC) on a Seiko Instruments SSC 5200 DSC. Heating and cooling rates of 10 K/min were used, and T_g was taken as the midpoint of the transition in the second heating curve. The T_g's for hhPP, PIB, and the 30% hhPP/70% PIB blend are 253, 203 K, and 217 K, respectively.

Dielectric Spectroscopy (DS). The complex permittivity $\epsilon^*(\omega) = \epsilon'(\omega) - i\epsilon''(\omega)$, where ϵ' and ϵ'' represent the dielectric permittivity and loss, respectively, and ω denotes angular frequency ($\omega = 2\pi f$, where f denotes frequency), was measured on a Novocontrol BDC-S system composed of a frequency response analyzer (Solartron Schlumberger FRA 1260) and a broad band dielectric convertor with an active sample cell containing six reference capacitors in the capacitance range of 25 pF−1000 pF. Experiments were conducted in the frequency range of 10^{-2} Hz−10^6 Hz for pure hhPP and between 10^{-1} Hz and 10^6 Hz for PIB and the blend by using a combination of three capacitors in the active cell. The resolution in the dielectric loss tangent $\tan \delta_d$ ($= \epsilon''/\epsilon'$) is about 2×10^{-4} between 10^{-1} and 10^5 Hz. Samples were prepared between 10 mm diameter gold-plated stainless steel plates separated by Teflon spacers. The sample cell was placed in a cryostat, and the accuracy in temperature control was ±0.1 K.

Saturated hydrocarbons like hhPP and PIB should have low dipole moments due to symmetric structure and small electronegativity differences between component atoms. In pure hhPP the amplitude of the α relaxation and the relaxation intensity is appreciable due to a small fraction (≅3%) formed from hydrogenation of asymmetric double bonds in the polydiene precursor. DS on hhPP/PIB blends contains a contribution from the dielectric response of hhPP segments, which are much more strongly dielectrically active than PIB.[30] For neat hhPP, signal averaging of three measurements per frequency was sufficient to get good signal-to-noise (S/N) ratio. For pure PIB and the hhPP/PIB blend, averaging of 30 or 35 measurements per frequency was performed to get reasonable S/N ratio with reasonable data statistics.

In the frequency domain, the Havriliak−Negami (HN) function [31] is frequently used to fit the dielectric relaxation spectrum.

$$\epsilon^*(\omega) = \epsilon_\infty + \frac{\Delta\epsilon}{[1 + (i\omega\tau_{HN})^\alpha]^\gamma} \tag{1a}$$

The term $\Delta\epsilon$ is the dielectric relaxation strength ($= \epsilon_0 - \epsilon_\infty$), where ϵ_0 and ϵ_∞ are the low-frequency (relaxed) and high-frequency (unrelaxed) values of the permittivity, respectively. The parameter τ_{HN} is the HN time scale, and α and γ are the HN shape parameters which satisfy $0 \le \alpha \le 1$ and $\alpha\gamma \le 1$. The parameters α and γ describe the symmetrical and asymmetrical broadening, respectively, of the distribution of relaxation times. In a log−log plot of ϵ'' vs ω, α and $\alpha\gamma$ give the low-frequency and high-frequency slopes, respectively, of the relaxation function. The characteristic time τ_{max} of the segmental relaxation process is related to τ_{HN}, as derived by Boersma et al. and Schroeter et al.[33]

$$\tau_{max} = \left[\frac{1}{\tau_{HN}}\left[\sin\frac{\alpha\pi}{2+2\gamma}\right]^{1/\alpha}\left[\sin\frac{\alpha\gamma\pi}{2+2\gamma}\right]^{-1/\alpha}\right]^{-1} \tag{1b}$$

To quantitatively compare the width of the relaxation time distributions measured by DS and NMR, it is important to know the interrelation between the frequency-domain HN shape parameters α and γ and the time-domain Kohlrausch−Williams−Watts (KWW) exponent β.[32] The KWW stretched exponential function is widely used to describe the time dependence of relaxation processes.

$$\Phi(t) = \exp\left[-\left\{\frac{t}{\tau_{KWW}}\right\}^\beta\right] \tag{2}$$

$\Phi(t)$ is the correlation function (of polarization fluctuations for DS), τ_{KWW} is the KWW time scale, and $0 < \beta \le 1$ that captures the deviation of the relaxation from pure exponential nature. Equation 2 can be equivalently described as the superposition of Debye relaxation processes.[32]

$$\Phi(t) = \exp\left[-\left\{\frac{t}{\tau_{KWW}}\right\}^\beta\right] = \int_{-\infty}^{\infty}\exp\left(-\frac{t}{\tau}\right)F(\ln\tau)\,d(\ln\tau) \tag{3}$$

$F(\ln\tau)$ is the distribution of relaxation times, defined in the log time scale rather than linear time scale because several decades of time are experimentally covered. $F(\ln\tau)$ can be used[32] to calculate ϵ''.

$$\epsilon''(\omega) = \Delta\epsilon\int_0^\infty F(\ln\tau)\frac{\omega\tau}{1+(\omega\tau)^2}\,d(\ln\tau) \tag{4}$$

It is customary to define an average relaxation time that corresponds to the integrated area of the KWW function, a result[32] based on the Gamma function, Γ.

$$\langle\tau\rangle = \frac{\tau_{KWW}}{\beta}\Gamma\left(\frac{1}{\beta}\right) \tag{5}$$

The relationships between the frequency-domain HN and time-domain KWW shape parameters have been derived by Alvarez et al.,[33] provided the following constraint is imposed on α and γ.

$$\gamma = 1 - 0.812(1-\alpha)^{0.387} \tag{6a}$$

The constraint enables a reduction in the number of free parameters in the HN model, and Alvarez et al.[33] have derived the following relationship contingent on eq 6a.

$$\beta = [\alpha\gamma]^{1/1.23} \tag{6b}$$

The values of $\Delta\epsilon$, α, γ, τ_{HN}, τ_{max}, and β for pure hhPP, pure PIB, and the hhPP/PIB blend at T_g, $T_g + 10$ K, and $T_g + 3$ K, respectively, are shown in Table 1. Equation 6a was used as a constraint during the HN fits to data. The HN α and γ parameters were thus converted[33] to the KWW β's using eq 6b.

DS data at various temperatures for pure hhPP and pure PIB are shown in Figures 2 and 3, respectively. In the experimental frequency window, hhPP shows a strong α-relaxation in its dielectric response (see Figure 2). The α-relaxation broadens as the temperature is lowered toward T_g. In PIB, both a high-frequency β-relaxation (observed most clearly below T_g, but also distinct in its presence as an upturn in ϵ'' at low temperatures/high frequencies in Figure 3) and the

Table 1. Havriliak–Negami Parameters $\Delta\epsilon$, α, γ, τ_{HN}, τ_{max}, β, and $\Gamma(1/\beta)/\beta$ of Pure PIB (at T_g + 10 K = 213 K), Pure hhPP (at T_g = 253 K), and 30% hhPP/70% PIB Blend (at T_g + 3 K = 222 K)[a]

	$\Delta\epsilon$	α	γ	τ_{HN} (s)	τ_{max} (s)	β	$\Gamma(1/\beta)/\beta$
PIB	5.05×10^{-3}	0.59	0.42_5	0.15	3.9×10^{-2}	0.33	6.3
hhPP	0.1575	0.53	0.39_3	20	3.79	0.28	19
30% hhPP/70% PIB	1.875×10^{-2}	0.36	0.31_6	10	0.293	0.154	287.8

[a] Equation 6a links γ and α, and eq 6b gives β.

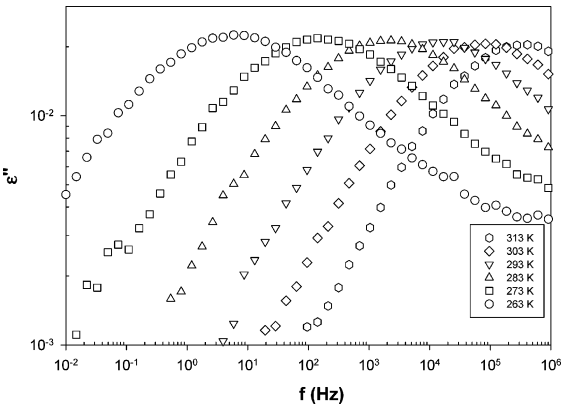

Figure 2. Frequency dependence of dielectric loss for pure hhPP at six temperatures.

α-relaxation were observed in the dielectric spectrum, in agreement with the experimental results of Richter et al.[34] Instrumental resolution effects also influence the increase in ϵ'' (and tan δ_d). The maximum in the PIB ϵ'' is rather small ($\epsilon''_{max} \approx 10^{-3}$), as expected for a symmetric molecule with a small dipole moment and somewhat smaller than previously reported by Richter et al.[34] However, we have compared our τ_{max} data to those of Richter et al.[34] and found excellent agreement between the data sets. A comparison of ϵ''_{max} for hhPP (Figure 2) and PIB (Figure 3) indicates that ϵ''_{max} in hhPP is about a factor of 20 larger than ϵ''_{max} in PIB, leading us to conclude that DS on hhPP/PIB blends is sensitive primarily to the segmental dynamics of hhPP segments in the blend.

DS data on the blend are shown in Figure 4. The segmental relaxation distribution is much broader in the blend than in the pure components. Such broadening has long been associated with concentration fluctuations[20] before the more recent attempts[11,14,19,21] to predict changes in dynamics upon blending.

NMR. Spin–lattice relaxation time (T_1) measurements were made using ^{2}H and ^{13}C NMR and the standard inversion recovery experiment. Two spectrometers were used at two different field strengths: a Varian Inova 400 wide bore and a Varian Mercury 200. For ^{2}H NMR the frequencies are 61.4 MHz and 30.7 MHz, respectively, while for ^{13}C NMR the frequencies are 100 MHz and 50 MHz, respectively. ^{13}C data on pure PIB were taken from the literature[35] while ^{13}C data on PIB in the blend are reported here. ^{13}C data on pure hhPP are reported here while ^{2}H data were acquired on deuterated hhPP in the blend.

For the ^{13}C data on PIB in the blend, a three-parameter fit based on Varian software was used to determine T_1 from the inversion recovery data. For the pure hhPP, each peak in the spectrum is split into a doublet because of the presence of about equal amounts of threo and erythro sequences. At lower temperatures and at the lower field strength, the two peaks overlap and deconvolution followed by off-line processing was used to determine T_1 values for individual peaks. At higher temperatures and at higher field strength, the peaks were sufficiently resolved so that the data could be analyzed directly using the manufacturer's software. The threo and erythro sequences had equal T_1 values within experimental error (±10%), and so only a single value is reported. Only the methylene data are reported, since they are least affected by nonbonded carbon proton dipolar interactions. The ^{2}H data on hhPP indicated that deuterons were present both in the methyl groups and on the backbone. However, the resonances strongly overlapped so that deconvolution was difficult. The methyl group deuterons had a spin–lattice relaxation time that was about an order of magnitude larger than the deuterons attached to the backbone (methylene and methine), enabling a double-exponential fit of the inversion recovery data to separately determine both times. An example of the recovery curve for the integrated intensity of all the deuterons is shown in Figure 5 along with a double-exponential fit. The analysis indicates that 40% of the deuterons are located on the backbone. The percentage of backbone and methyl deuterons was confirmed by dilute solution deuterium NMR on the deuterated hhPP. Since the associated short T_1's are the data of interest, only the initial part of the recovery curve was fitted to obtain a more accurate value of this component. The initial part of the recovery was considered to be about 3 times the short T_1 in duration. The shorter backbone deuterium T_1's have an error of ±10%.

^{13}C spin–lattice relaxation times for the methylene carbons in pure hhPP are shown in Figure 6 as a function of temperature at two Larmor frequencies. Similarly, spin–lattice relaxation times for the methylene carbons in pure PIB (taken from ref 35) are shown in Figure 7 as a function of temperature at three Larmor frequencies. For deuterated hhPP in the blend, ^{2}H spin–lattice relaxation times are shown in Figure 8 as a function of temperature at two Larmor frequencies, and ^{13}C spin–lattice relaxation times for PIB in the same blend are shown in Figure 9 as a function of temperature at two Larmor frequencies.

The ^{13}C spin–lattice relaxation time can be written in terms of the spectral densities, J's, and the dipole–dipole interaction that depends on the internuclear distance, r, and the gyromagnetic ratios, γ_C and γ_H, for carbon and hydrogen, respectively.[22] The value of the constant K is 2.28×10^9.

$$\frac{1}{T_1} = Kn[J(\omega_H - \omega_C) + 3J(\omega_C) + 6J(\omega_H + \omega_C)] \quad (7)$$

$$K = \frac{\gamma_C^2 \gamma_H^2 \hbar^2}{10 r_j^6} \quad (8)$$

The spectral densities are functions of the Larmor frequencies for carbon and hydrogen, ω_C and ω_H. The number of directly bonded protons is n (= 2 for the methylene carbon in PIB). A similar equation can be written for ^{2}H spin–lattice relaxation.

$$\frac{1}{T_1} = \frac{3}{10}\pi^2(e^2qQ/h)^2[J(\omega_D) + 4J(2\omega_D)] \quad (9)$$

The quadrupole coupling constant e^2qQ/h is set at 172 kHz[22] for the deuterons on the backbone carbons of hhPP. The spectral density is the Fourier transform of the orientation autocorrelation function $G(t)$.

$$J(\omega) = \frac{1}{2}\int_{-\infty}^{\infty} G(t) \exp(-i\omega t)\, dt \quad (10)$$

$G(t)$ is defined as follows:

$$G(t) = \frac{3}{2}\langle \cos^2 \theta(t) \rangle - \frac{1}{2} \quad (11)$$

$\theta(t)$ is the angle between the C–H or C–D bond relative to time $t = 0$.

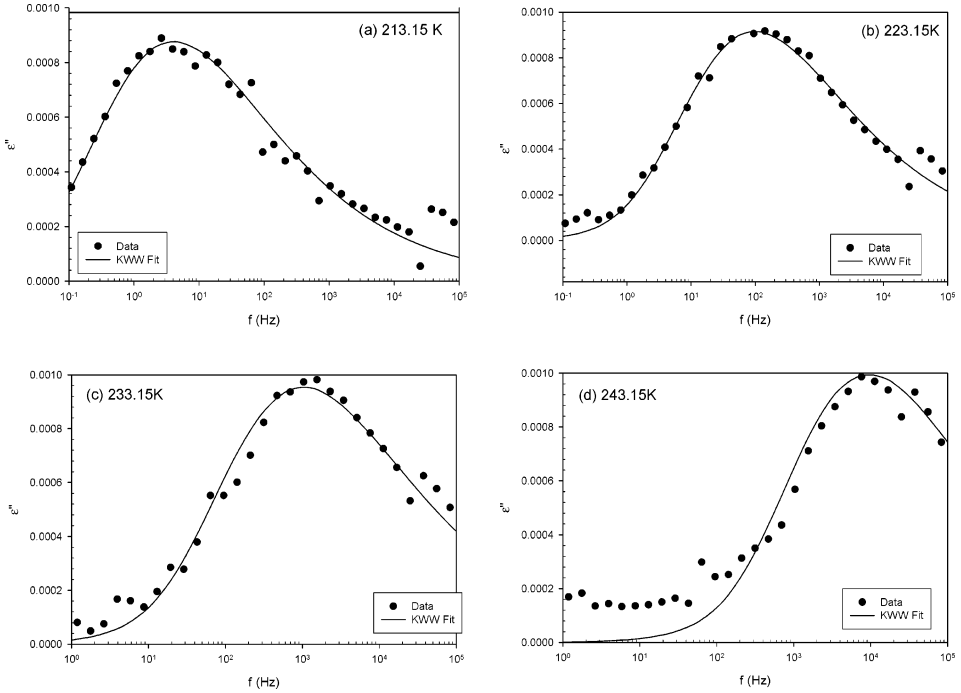

Figure 3. Frequency dependence of dielectric loss of pure PIB at (a) 213 K, (b) 223 K, (c) 233 K and (d) 243 K. The points are experimental data, while the curves are KWW fits corresponding to the fit parameters listed in Table 1.

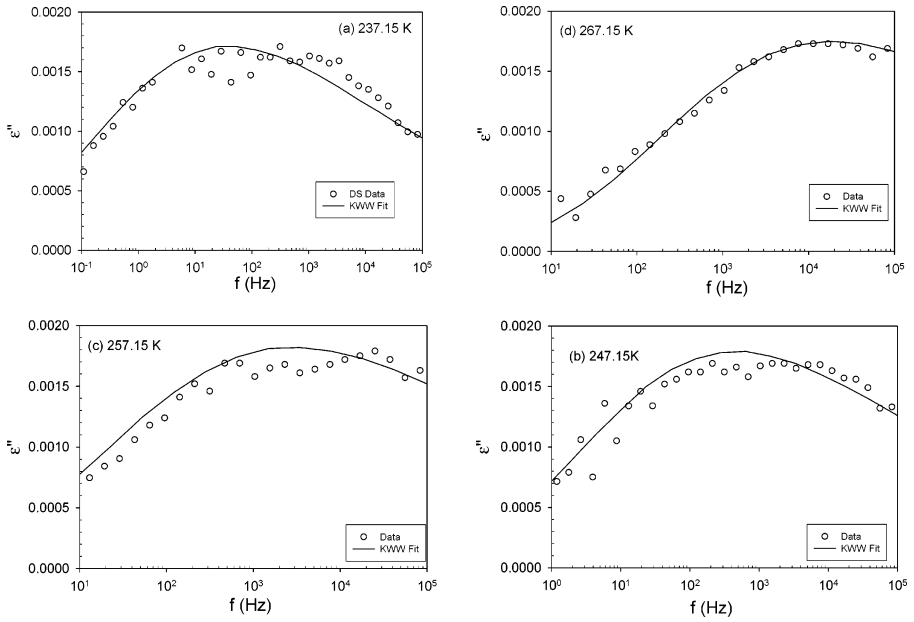

Figure 4. Frequency dependence of dielectric loss of 30% hhPP/70% PIB blend at (a) 237 K, (b) 247 K, (c) 257 K and (d) 267 K. The points are experimental data, while the curves are KWW fits corresponding to the fit parameters listed in Table 1.

The correlation function used in this interpretation is the modified KWW form.

$$G(t) = a_{\text{lib}} \exp\left(-\frac{t}{\tau_{\text{lib}}}\right) + (1 - a_{\text{lib}}) \exp\left[-\left(\frac{t}{\tau_{\text{seg}}}\right)^{\beta}\right] \quad (12)$$

This form has been used before to interpret spin−lattice relaxation in homopolymers and polymer blends.[22,23] This autocorrelation function assumes two motions contribute to spin−lattice relaxation: librational motion and segmental dynamics. The amplitude of the librational motion is controlled by the parameter a_{lib} and the relaxation time for librational motion is τ_{lib}. Since the fit to the data is insensitive to the choice of the librational correlation time as long as it is much shorter than the correlation time for segmental motion, τ_{lib} is set to 0.1 ps for all cases.

The parameters describing segmental motion are the segmental time scale τ_{seg} and the width parameter β. In the modified KWW function, the distribution of segmental correlation times is controlled by the choice of β. VFTH temperature dependence[22,23] is assumed.

$$\log \frac{\tau_{\text{seg}}}{\tau_{\infty}} = \frac{B}{T - T_{\infty}} \quad (13)$$

T_{∞} is the Vogel temperature, τ_{∞} is a time scale, and the parameter B is an activation energy divided by the Boltzmann constant.

For the pure components and each component in the blend, a set of values of τ_{∞}, B, and T_{∞} is determined by fitting the temperature dependence of the spin−lattice relaxation

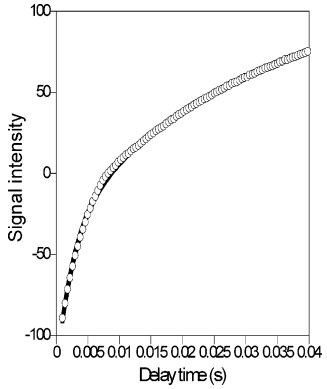

Figure 5. ^{2}H inversion recovery curve for hhPP at 30.7 MHz and $T = 363$ K. The points were fit to a double-exponential function (solid curves) to determine two values of the spin−lattice relaxation time associated with deuterons in the methyl group and deuterons on the backbone.

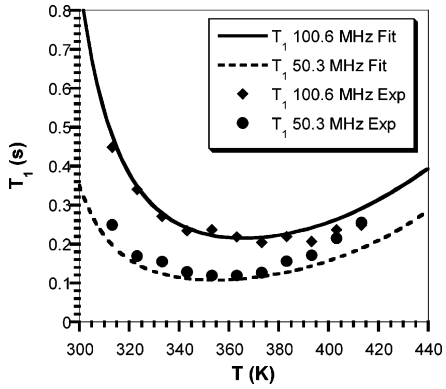

Figure 6. Temperature dependence of ^{13}C spin−lattice relaxation times for pure hhPP.

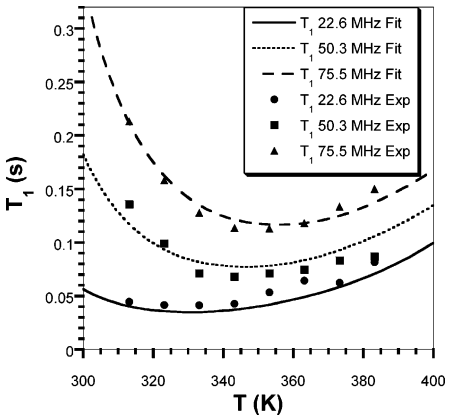

Figure 7. Temperature dependence of ^{13}C spin−lattice relaxation times for pure PIB.

data. To get a characteristic time scale $\tau_{seg,c}$ for segmental dynamics measured by NMR, we use the integral of the segmental part of the correlation function.

$$\tau_{seg,c} = \frac{\tau_{seg}}{\beta}\Gamma\left(\frac{1}{\beta}\right) \tag{14}$$

This is the same form as the average correlation time used to summarize the dielectric data (see eq 5). The fits of the spin−lattice relaxation data determined by this procedure are shown along with the data in Figures 6−9. The parameters a_{lib}, τ_∞, B, β, and T_∞, produced by the fitting procedure, are listed in Table 2 along with the associated uncertainties. Note that τ_∞ and τ_{lib} were both held fixed at 0.1 ps in the interpretation to obtain a better comparison of the remaining parameters

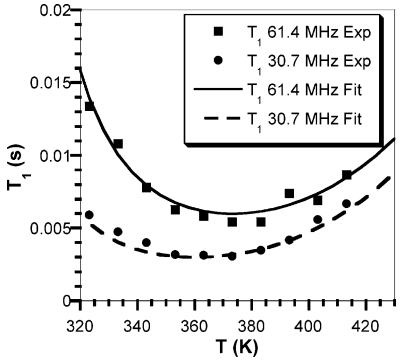

Figure 8. Temperature dependence of ^{2}H spin−lattice relaxation times for hhPP in the 30% hhPP/70% PIB blend.

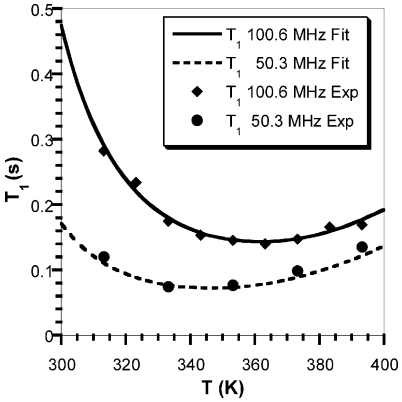

Figure 9. Temperature dependence of ^{13}C spin−lattice relaxation times for PIB in the 30% hhPP/70% PIB blend.

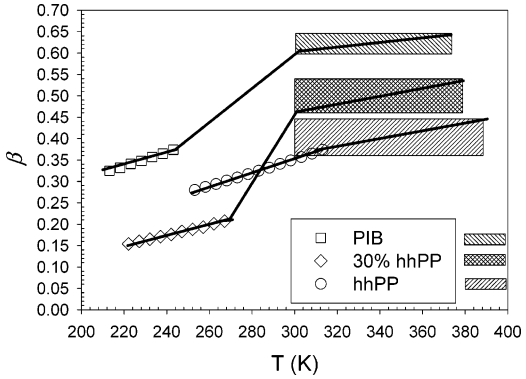

Figure 10. Temperature dependence of the KWW β parameter for pure PIB, pure hhPP, and the 30% hhPP/70% PIB blend. Symbols are from DS and shaded boxes represent the range of possibilities from NMR. The curves are merely guides to the eye.

associated with segmental motion. In each set of spin−lattice relaxation data as a function of temperature (pure hhPP, pure PIB, hhPP in the blend, and PIB in the blend), the data at all Larmor frequencies were fit simultaneously.

Discussion

Since both the NMR data and DS data are interpreted in terms of a KWW distribution for segmental correlation times, the time scales and width parameters can be meaningfully compared. The broadening is reflected in the KWW β, which is plotted as a function of temperature for pure PIB, pure hhPP, and the 30% hhPP/70% PIB blend in Figure 10, using both DS and NMR data. In all cases β decreases with decreasing temperature, meaning that *the segmental distribution broadens with decreasing temperature*. In PIB β at high

temperatures is somewhat larger than for common flexible polymers, as noted previously.[34,36] Little change in breadth is noted over the limited temperature range studied, and so a constant value is sufficient, which changes at the lowest temperatures of the DS data. A restricted trans + to trans process is proposed[34] in PIB, which overlaps the overall segmental process. In our interpretation this restricted motion is ignored, but this process could influence the width parameter or the part of the relaxation that is ascribed to libration. The β for pure hhPP, as determined from the HN parameters from fits to DS data (vide eqs 6a and 6b) is in good agreement with the β value determined from NMR: $\beta = 0.28$ at $T = 253$ K, and it steadily increases to reach 0.37 at $T = 318$ K. The temperature dependence of β for hhPP is typical of amorphous flexible polymers. The hhPP backbone contains erythro and threo sequences, and we are averaging over this structural variation, which may contribute to the broader value for the distribution.

The temperature dependence of β in the blend is unusual. The DS data show β smaller than either of the pure components, as seen for all miscible polymer blends with weak interactions between the components, which is believed to be related to concentration fluctuations in miscible blends.[14,19] However, the NMR estimations of β for hhPP in the blend are considerably larger, falling between the values for pure PIB and pure hhPP. The ^{13}C spin−lattice relaxation times from NMR reflect fast motions at high temperatures and do not extend to lower temperatures where β becomes small. The β determined from HN parameters fit to the hhPP/PIB blend data varies from 0.15 at $T = 227$ K to 0.19 at $T = 252$ K, reflecting significant broadening of the relaxation time distribution of hhPP in the blend.

The combined NMR and DS relaxation time data are shown in Figure 11. The NMR times for the pure components and the components in the blend are $\tau_{seg,c}$ calculated from eq 14. Two blend dielectric time scales are shown in Figure 11: τ_{max} and $\langle\tau\rangle$. The τ_{max} values for the blend and pure components were calculated from eq 1b. The average time scale $\langle\tau\rangle$ was calculated using the KWW β derived from the HN fits to the blend (plotted in Figure 10), expressing the KWW function as an integral over the distribution of relaxation times (eq 3) and adjusting the τ_{KWW} until the ϵ'' calculated using the integral over the distribution of relaxation times gave a peak at $1/\tau_{max}$ (eq 4). An average relaxation time $\langle\tau\rangle$ was then calculated from τ_{KWW} using eq 5. The calculation of $\langle\tau\rangle$ is necessary because $\epsilon''(\omega)$ in the blend is anomalously broad. For the pure components, whose $\epsilon''(\omega)$ spectra are much narrower than the blend, τ_{max} and $\langle\tau\rangle$ are within a factor of 2 or so of each other. In the blend the relaxation time distribution is much broader near the T_g than at high temperatures accessed by NMR data, as expected. In this situation τ_{max} is much smaller than $\langle\tau\rangle$ (see Figure 11). The DS experiments are critical, as they selectively probe hhPP segmental dynamics near T_g. We discuss these issues in more detail and consider the implications of these data for the LM model.[21]

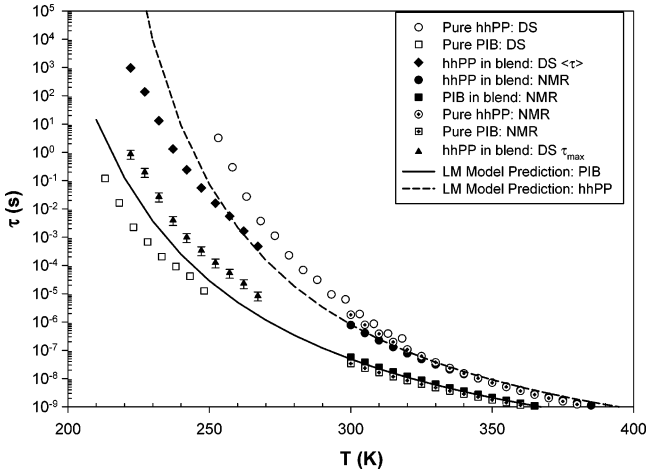

Figure 11. Temperature dependence of segmental correlation times from DS and NMR data for hhPP, PIB, and the 30% hhPP/70% PIB blend. DS data on the pure components and the blend are τ_{max}. For the blend, dielectric response $\langle\tau\rangle$ is also calculated using eq 5 and the β in Table 1 and plotted above. In both DS and NMR, the blend relaxation time reflects motion of hhPP. For the hhPP LM prediction, $\phi_{self} = 0.75$.

Some qualitative aspects of the local dynamics readily fall out of the spin−lattice relaxation data and the DS data even before any quantitative interpretation. At $f \approx 1$ Hz, the loss maxima of pure hhPP and pure PIB are separated by 50 K, consistent with the separation in their DSC T_g's. As temperature and frequency are increased, the separation of the dielectric loss maxima decreases because of the weak temperature dependence of the PIB data and the stronger temperature dependence of the hhPP data. In the spin−lattice relaxation data, the T_1 minimum occurs at a correlation time of about 1 ns. For pure hhPP at a Larmor frequency of 50 MHz, the minimum is at 365 K in Figure 6, while for PIB the minimum at the same frequency in Figure 7 is about 345 K. At these higher frequencies, the temperature separation of the dynamics is about 20 K, again showing the narrowing separation between the dynamics of the two pure polymers as temperature is increased. In Figure 8, the deuterium T_1 minimum at 61.4 MHz for hhPP in the blend is about 365 K, which is close to the minimum in pure hhPP. Similarly in Figure 9, the minimum for PIB in the blend is still about 345 K, which is the same as for pure PIB. At these higher temperatures and higher frequencies the dynamics of PIB and hhPP are close as pure components and *change little upon* blending, in contrast with the situation at lower temperatures where there is a larger separation of the intrinsic dynamics of the pure components.

This finding is consistent with those on PI/PVE blends where similar observations have been made on the differences in the segmental dynamics of PI and PVE at low temperatures close to[10,11] the blend T_g. According to the NMR data, the hhPP segments speed up a little upon blending, while the PIB dynamics slow down. These two changes bring the dynamics of the pure polymers closer together upon blending, in agreement

Table 2. Segmental Motion Parameters a_{lib}, β, τ_∞, B, and T_∞ for Pure hhPP, Pure PIB, and These Two as Components of the 30% hhPP/70% PIB Blend (Determined from NMR Data)

	a_{lib}	β	τ_∞ (ps)	B (K)	T_∞ (K)
pure PIB	0.31 ± 0.04	0.62 ± 0.02	0.1 ± 0.02	820 ± 30	150 ± 10
PIB (blend)	0.26 ± 0.03	0.60 ± 0.04	0.1 ± 0.05	775 ± 25	160 ± 5
pure hhPP	0.29 ± 0.03	0.40 ± 0.04	0.1 ± 0.01	606 ± 50	210 ± 10
hhPP (blend)	0.07 ± 0.03	0.50 ± 0.02	0.1 ± 0.05	730 ± 50	188 ± 5

Table 3. VFTH Parameters τ_∞, B, and T_∞ for Pure hhPP and Pure PIB (NMR and DS Data Were Combined Here)

	τ_∞ (s)	B (K)	T_∞ (K)
pure hhPP	1.36×10^{-13}	738	198
pure PIB	2.61×10^{-13}	793	142

with conventional wisdom and the results of NMR,[10,11,22] neutron spin echo,[37] and fluorescence anisotropy decay experiments[38] on PI/PVE blends which clearly show that PI (the low-T_g component) is *slowed down* upon blending with PVE (high-T_g component), while PVE is *speeded up* in the blend. In the PI/PVE blend system, the local dynamics of the components have similar temperature dependencies, and the separation of the time scale of the dynamics does not change so much with temperature.[10,11,18−22] The unusual temperature dependence of PIB changes the situation in its blend with hhPP.

To extract VFTH parameters that universally describe the segmental dynamics of the pure components, we combine the NMR and DS time scales for pure hhPP and for pure PIB and perform fits of the VFTH equation (eq 13) to the combined data. The VFTH parameters extracted by this procedure for the pure components are listed in Table 3. For both pure components, T_∞ determined by combination of NMR and DS data are in good agreement with T_∞ determined only from the NMR data, and it is indeed possible to capture the temperature dependence of the dynamics probed by NMR and DS in the pure components by a single set of VFTH parameters. As pointed out by Richter et al.,[34] PIB is one of the least fragile polymeric glass-formers.[39] The VFTH temperature dependence of PIB involves a large B and a small T_∞, indicating a more Arrhenius temperature dependence than hhPP, which has a smaller (and more typical) value of B. These differences in the temperature dependence of the pure components explain the narrowing of the separation of the dynamics with increasing temperature. Upon blending, the temperature dependencies of the two components become more similar, which leads to a separation of the dynamics relative to the pure polymers at low temperature.

One of the main goals of this study is to characterize and understand the changes in component dynamics induced by blending. The LM model[21] provides a method for calculating an effective Vogel temperature, $T_{\infty,\mathrm{eff}}$, for each component in a blend. A composition-dependent T_∞ is assumed with the key factor being the effective concentration, ϕ_{eff}, experienced by each component on the scale of the Kuhn length. Each component experiences on average a higher ϕ_{eff} than the bulk concentration (ϕ) due to chain connectivity. The self-concentration, ϕ_{self}, is a measure of this effect, and it is calculated on the basis of a volume taken as the cube of the Kuhn length, b.

$$b = \frac{C_\infty l}{\cos(\theta/2)} \tag{15}$$

C_∞ is Flory's characteristic ratio, $l = 1.54$ Å is the backbone bond length, and $\theta = 68°$ is the backbone bond angle.

$$\phi_{\mathrm{self}} = \frac{C_\infty M_0}{k\rho N_{\mathrm{Av}} b^3} \tag{16}$$

M_0 is the repeat unit molar mass, k is the number of backbone bonds per repeat unit, ρ is the density, and N_{Av} is Avogadro's number. The ϕ_{eff}, which depends on ϕ_{self} and ϕ, is the peak in the distribution of compositions around a monomer segment, and hence it corresponds to the peak relaxation time $\tau_{\max}$.

$$\phi_{\mathrm{eff}} = \phi_{\mathrm{self}} + (1 - \phi_{\mathrm{self}})\phi \tag{17}$$

The ϕ_{eff} is used to calculate $T_{\infty,\mathrm{eff}}$ using the Fox equation.

$$T_{\infty,\mathrm{eff}} = T_\infty(\phi_{\mathrm{eff}}) = \left(\frac{\phi_{\mathrm{eff}}}{T_{\infty,\mathrm{A}}} + \frac{1 - \phi_{\mathrm{eff}}}{T_{\infty,\mathrm{B}}}\right)^{-1} \tag{18}$$

For hhPP[40] $C_\infty = 6.1$ and $\rho = 0.878$ g cm^{-3}, while for PIB[41] $C_\infty = 6.7$ and $\rho = 0.918$ g cm^{-3} (at 298 K). Using these values, we determine $\phi_{\mathrm{self}} = 0.16$ and $\phi_{\mathrm{self}} = 0.17$ for hhPP and PIB, respectively. Using the VFTH equation (with pure component B's and T_∞'s from Table 3) to describe the temperature dependence of relaxation time, we calculate the LM model predictions for the relaxation times of hhPP and PIB in the blend (see Figure 11).

To fit the LM model to the experimental data on PIB segmental correlation times in the blend, the prefactor τ_∞ in the VFTH equation for PIB in the blend had to be adjusted to 2.0×10^{-13} s from 2.61×10^{-13} s (the latter is the pure PIB τ_∞, shown in Table 3). The LM model prediction for PIB in the blend was calculated with $\phi_{\mathrm{self}} = 0.17$, and the LM model prediction with this ϕ_{self} and the adjusted τ_∞ is in good agreement with data over the limited range of temperatures studied by NMR.

A much more stringent test of the LM model is afforded by the data on hhPP in the blend, which are *much closer to* $T_{\infty,\mathrm{eff}}$. This combination of NMR and DS data in the blend can be well described by a single VFTH equation when both types of data are summarized by an average correlation time calculated in the same way from eqs 5 and 14. In DS a broad unimodal distribution is observed in the blend, and extracting the relevant segmental correlation times is not a simple task. The $\langle\tau\rangle$, which is a linear average, is weighted toward the *slow end* of the distribution (and hence it cannot be compared to the time scale calculated using ϕ_{eff}), while $\tau_{\max}$ is weighted toward the *fast end* of the distribution. To fit the LM model to the NMR correlation times of hhPP in the blend, we use $\phi_{\mathrm{self}} = 0.75$, making $\phi_{\mathrm{eff}} = 0.825$ (whereas the LM model predicts $\phi_{\mathrm{self}} = 0.16$ and $\phi_{\mathrm{eff}} = 0.41$ for hhPP) and $\tau_\infty = 3 \times 10^{-13}$ s. However, even with this adjusted ϕ_{self}, the LM model does not fit the $\langle\tau\rangle$ from DS data on hhPP in the blend.

The origins of this discrepancy at low temperatures between LM model predictions and data may lie in the assumption of a constant cooperative length scale in the LM model. Kant et al.[42] have demonstrated (by reverse fitting the LM model to experimental data on component segmental relaxation times in various miscible blends) that while the low-T_g component in miscible blends behaves in accord with the LM assumption of a temperature invariant cooperative length scale, the cooperative length scale of the high-T_g component *increases monotonically with decreasing temperature*. Since the length scale increases with decreasing temperature, the self-composition must decrease, making the hhPP segmental correlation time systematically smaller than the prediction based on the temperature invariance assumption for the cooperative length scale of the high-T_g component in the LM model. The erroneous LM predictions of the segmental and terminal dynamics of

the high-T_g component are most amplified at low temperatures, a regime that has been neglected in recent tests[43,44] of the LM model. Since the LM model does not make any predictions for the change in the breadth of the component segmental relaxation time distributions upon blending, we are unable to offer any rationalization from the LM standpoint.

Another possibility that may help explain why the LM model fails to fit the hhPP segmental correlation times is that the mixing rule used for T_∞, the Fox equation (eq 18) may not be most appropriate.[45] The proper choice of a blending law may help the LM prediction for the high-T_g component agree perfectly with the τ_{max}.

Conclusions

The local dynamics of pure PIB, pure hhPP, and their dynamics in an hhPP/PIB blend are well characterized by the combination of NMR and DS experiments over wide ranges of time and temperature. The unusual temperature dependence of pure PIB segmental dynamics leads to a closer approach to the local dynamics of pure hhPP as temperature is raised. Thus, although there is a 50 K separation in pure component T_g's (corresponding to several decades of separation of the segmental dynamics), the dynamics differ only by half a decade in time at the highest temperatures studied by NMR. For 300 K < T < 400 K little shift in the dynamics is produced by blending, but as temperature is lowered the separation between the local motion of the pure polymers and the same polymer in the blend increases. The shift upon blending of the PIB local motions is described well by the LM model prediction over the limited range of temperatures studied by NMR while the shift in hhPP dynamics is at variance with the model prediction.

Acknowledgment. The Clark Univ group acknowledges the financial support of the National Science Foundation (NSF) Grant DMR-0209614. The Penn. State Univ group acknowledges NSF grant DMR-9977928 and an NSF travel grant (INT-9800092). J.A.P. thanks his colleagues (especially Prof. George Fytas) at FORTH-IESL for their warm hospitality during his visits. The authors thank Professor Mark Ediger for a critical reading of the manuscript.

References and Notes

(1) Paul, D. R.; Bucknall, C. B. *Polymer Blends*; Wiley-Interscience: New York, 2000; Vols. 1 and 2.
(2) Green, P. F.; Kramer, E. J. *Macromolecules* **1986**, *19*, 1108−1114.
(3) Composto, R. J.; Kramer, E. J.; White, D. M. *Polymer* **1990**, *31*, 2320−2328.
(4) Green, P. F.; Adolf, D. B.; Gilliom, L. R. *Macromolecules* **1991**, *24*, 3377−3382.
(5) Composto, R. J.; Kramer, E. J.; White, D. M. *Macromolecules* **1992**, *25*, 4167−4174.
(6) Chin, Y. H.; Zhang, C.; Wang, P.; Inglefield, P. T.; Jones, A. A.; Kambour, R. P.; Bendler, J. T.; White, D. M. *Macromolecules* **1992**, *25*, 3031−3038.
(7) Chin, Y. H.; Inglefield, P. T.; Jones, A. A. *Macromolecules* **1993**, *26*, 5372−5378.
(8) Green, P. F. *J. Non-Cryst. Solids* **1994**, *172*, 815−822.
(9) Kim, E.; Kramer, E. J.; Wu, W. C. Garett, P. D. *Polymer* **1994**, *35*, 5706−5715.
(10) Chung, G. C.; Kornfield, J. A.; Smith, S. D. *Macromolecules* **1994**, *27*, 964−973.
(11) Chung, G. C.; Kornfield, J. A.; Smith, S. D. *Macromolecules* **1994**, *27*, 5729−5741.
(12) McGrath, K. J.; Roland, C. M. *J. Non-Cryst. Solids* **1994**, *172*, 891−896.
(13) Kim, E.; Kramer; E. J.; Osby, J. O. *Macromolecules* **1995**, *28*, 1979−1989.
(14) Kumar, S. K.; Colby, R. H.; Anastasiadis, S. H.; Fytas, G. *J. Chem. Phys.* **1996**, *105*, 3777−3788.
(15) Lartigue, C.; Guillermo, A.; Cohen-Addad, J. P. *J. Polym. Sci., Part B: Polym. Phys.* **1997**, *35*, 1095−1105.
(16) Schantz, S. *Macromolecules* **1997**, *30*, 1419−1425.
(17) Schantz, S.; Veeman, W. S. *J. Polym. Sci., Part B: Polym. Phys.* **1997**, *35*, 2681−2688.
(18) Saxena, S.; Cizmeciyan, D.; Kornfield, J. A. *Solid State Nucl. Magn. Reson.* **1998**, *12*, 165−181.
(19) Kamath, S.; Colby, R. H.; Kumar, S. K.; Karatasos, K.; Floudas, G.; Fytas, G.; Roovers, J. E. L. *J. Chem. Phys.* **1999**, *111*, 6121−6128.
(20) Shears, M. F.; Williams, G. *J. Chem. Soc., Faraday Trans. 2* **1973**, *69*, 608−621.
(21) Lodge, T. P.; McLeish, T. C. B. *Macromolecules* **2000**, *33*, 5278−5284.
(22) Min, B. C.; Qui, X. H.; Ediger, M. D. Pitsikalis, M.; Hadjichristidis, N. *Macromolecules* **2001**, *34*, 4466−4475.
(23) Lutz, T. R.; He, Y.; Ediger, M. D.; Cao, H.; Lin, G.; Jones, A. A. *Macromolecules* **2003**, *36*, 1724−1730.
(24) Krishnamoorti, R.; Graessley, W. W.; Fetters, L. J.; Garner, R. T.; Lohse, D. J. *Macromolecules* **1995**, *28*, 1252−1259.
(25) White, J. L.; Lohse, D. J. *Macromolecules* **1999**, *32*, 958−960.
(26) Angell, C. A.; Monnerie, L.; Torell, L. M. *Symp. Mater. Res. Soc.* **1991**, *215*, 3−9.
(27) Boyd, R. H.; Pant, P. V. K. *Macromolecules* **1991**, *24*, 6325−6331.
(28) Pant, P. V. K.; Boyd, R. H. *Macromolecules* **1992**, *25*, 494−495.
(29) Pant, P. V. K.; Boyd, R. H. *Macromolecules* **1993**, *26*, 679−686.
(30) Pathak, J. A. Miscible Polymer Blend Dynamics. Doctoral Dissertation, The Pennsylvania State University, University Park, PA, 2001.
(31) Havriliak, S.; Negami, S. *Polymer* **1967**, *8*, 161−205.
(32) See: Kremer, F.; Schönhals, A. In *Broadband Dielectric Spectroscopy*; Kremer, F., Schönhals, A., Eds.; Springer-Verlag: Berlin, 2003; Chapter 3.
(33) Schroeter, K.; Unger, R.; Reissig, S.; Garwe, F.; Kahle, S.; Beiner, M.; Donth, E. *Macromolecules* **1998**, *31*, 8966−8972. Boersma, A.; van Turnhout, J.; Wuebbenhorst, M. *Macromolecules* **1998**, *31*, 7453−7460. Alvarez, F.; Alegria, A.; Colmenero, J. *Phys. Rev. B* **1991**, *44*, 7306−7312; ibid. **1993**, *47*, 125−130.
(34) Richter, D.; Arbe, A.; Colmenero, J.; Monkenbusch, M.; Farago, B.; Faust, R. *Macromolecules* **1998**, *31*, 1133−1143.
(35) Bandis, A.; Wen, W. Y.; Jones, E. B.; Kaskan, P.; Zhu, Y.; Jones, A. A.; Inglefield, P. T. *Polym. Prepr. (Am. Chem. Soc., Div. Polym. Chem.)* **1994**, *35* (1), 427−428.
(36) Ngai, K. L.; Plazek, D. J.; Bero, C. A. *Macromolecules* **1993**, *26*, 1065−1071.
(37) Hoffmann, S.; Willner, L.; Richter, D.; Arbe, A.; Colmenero, J.; Farago, B. *Phys. Rev. Lett.* **2000**, *85*, 772−775.
(38) Adams, S.; Adolf, D. B. *Macromolecules* **1999**, *32*, 3136−3145.
(39) Böhmer, R.; Ngai, K. L.; Angell, C. A.; Plazek, D. J. *J. Chem. Phys.* **1993**, *99*, 4201−4209.
(40) Hattam, P.; Gauntlett, S.; Mays, J. W.; Hadjichristidis, N.; Young, R. N.; Fetters, L. J. *Macromolecules* **1991**, *24*, 6199−6209.
(41) Fetters, L. J.; Lohse, D. J.; Richter, D.; Witten, T. A.; Zirkel, A. *Macromolecules* **1994**, *27*, 4639−4647.
(42) Kant, R.; Kumar, S. K.; Colby, R. H. *Macromolecules* **2003**, *36*, 10087−10094.
(43) Haley, J. C.; Lodge, T. P.; He, Y.; Ediger; M. D.; von Meerwall, E. D.; Mijovic, J. *Macromolecules* **2003**, *36*, 6142−6151.
(44) He, Y.; Lutz, T.; Ediger, M. D. *J. Chem. Phys.* **2003**, *119*, 9956−9965.
(45) Colby, R. H.; Lipson, J. E. G. *Macromolecules* **2005**, *38*, 4919.

MA048224F